

³⁸J. E. Zimmerman, P. Thiene, and J. T. Harding, *J. Appl. Phys.* **41**, 1572 (1970).

³⁹J. E. Zimmerman and J. E. Mercereau, *Phys. Rev. Letters* **13**, 125 (1964).

PHYSICAL REVIEW B

VOLUME 4, NUMBER 5

1 SEPTEMBER 1971

Magnetoacoustic Wave in an Electron-Hole Gas—Bismuth

C. Guthmann, J. P. D'Haenens, and A. Libchaber

Groupe de Physique des Solides, Ecole Normale Supérieure, 24 rue Lhomond, Paris 5^e, France

(Received 19 October 1970)

This paper presents an experimental study in bismuth of the acoustic plasma wave at microwave frequencies. We have studied the coupling, in the presence of a dc magnetic field, of this wave to the Alfvén mode; experiments have been performed at two frequencies: 10 and 3 GHz. The 3-GHz transmission spectrometer devised by the authors shows very clearly the presence of the magnetoacoustic mode, while at 10 GHz hybrid and cyclotron resonances are mixed with the phenomenon studied. The electromagnetic theory of this phenomenon in the case of a collisionless isotropic plasma is recalled; the case of bismuth is then fully analyzed and compared with experiment. From the coupling of the two modes, $n\epsilon_0$ is obtained, where n is the carrier density and ϵ_0 the band overlap.

I. INTRODUCTION

Alfvén-wave propagation in bismuth has been extensively studied¹ since the original work of Buchsbaum and Galt.² Using compensated solid-state plasmas, McWhorter and May³ have tried, unsuccessfully, to discover evidence for acoustic waves, in the electron-hole gas. Yokota⁴ has studied the theoretical coupling of the compressional Alfvén mode with the magnetoacoustic wave in the presence of a magnetic field; this effect has been observed experimentally in bismuth by Lupatkin and Nanney⁵ and, more recently, by D'Haenens and Libchaber.⁶

In this paper a theoretical and systematic experimental study of the magnetoacoustic mode in bismuth is presented.

In Sec. II, the electromagnetic theory of this phenomenon allows the analysis of the effect of temporal and spatial dispersion on the wave spectrum. In the same section, the dispersion equation of the compressional Alfvén wave and of the magnetoacoustic mode is obtained in the complex case of bismuth, from the knowledge of the conductivity tensor for an ellipsoidal Fermi surface in the spatial-dispersion regime (Appendix B). An important result is derived: The quantity $n\epsilon_0$ (where n is the carrier density and ϵ_0 the band overlap energy) can be obtained experimentally.

In Sec. III, the experimental apparatus used is presented, in particular, the two-strip-resonators transmission spectrometer used at 3 GHz.

In Sec. IV, the theoretical and experimental results are presented and compared at two frequencies: 9.65 and 2.80 GHz. It is shown that at 2.8

GHz the magnetoacoustic mode appears very clearly, while at 10 GHz hybrid and cyclotron resonance are mixed with the phenomenon studied.

In Appendix A, it is recalled that the magneto-hydrodynamical model of the propagation and coupling of the compressional Alfvén wave with the acoustic wave can be applied to the collisionless plasma, when the direction of wave propagation is perpendicular to the magnetic field. This approach, a classical one for gaseous-plasma physicists does not yet seem to be widely known to solid-state physicists.

II. ELECTROMAGNETIC THEORY OF PROPAGATION OF COMPRESSIONAL ALFVÉN MODE AND ITS COUPLING WITH MAGNETOACOUSTIC MODE

In Sec. II A, we review the electromagnetic theory of the Alfvén and magnetoacoustic modes for an isotropic compensated plasma. In Sec. II B we study the limits of these results in the cyclotron-resonance ($\omega \sim \omega_c$) and nonlocal-dispersion ($qR \sim 1$) regime, where \vec{q} is the wave vector and R the cyclotron radius. Finally, in Sec. II C we present the theory of these modes for an anisotropic plasma like bismuth.

A. Electromagnetic Theory of Coupling of the Compressional Alfvén Mode with the Magnetoacoustic Mode

The electromagnetic theory of the coupling of the compressional Alfvén mode with the magnetoacoustic mode has been described by Yokota.⁴ Let us recall it briefly. Consider an isotropic degenerated compensated plasma gas with an electron (hole) Fermi energy ϵ_{Fe} (ϵ_{Fh}) and carrier density $n(n_e = n_h)$. The conductivity tensor, in a small spa-

tial-dispersion regime, is easily written in a power-series expansion up to $(qR)^2$ from Eq. (B5) of Appendix B. Let us define a right triad ($Oxyz$) with Oz parallel to \vec{B} , the applied static magnetic field. We are only interested in modes with an electrical polarization perpendicular to the magnetic field, and with \vec{q} parallel to Oy . Thus we need only the conductivity-tensor elements in a plane perpendicular to \vec{B} , which under the conditions

$$\omega \ll \omega_{ci}, \quad qR_i \ll 1 \quad (1)$$

are

$$\begin{aligned} \sigma_{xx}^i &= \frac{n_i e^2}{im_i \omega} \left(\frac{\omega^2}{\omega_{ci}^2} - \frac{2}{5} q^2 R_i^2 \right), \\ \sigma_{yy}^i &= \frac{n_i e^2}{im_i \omega} \frac{\omega^2}{\omega_{ci}^2}, \\ \sigma_{xy}^i &= \frac{n_i e^2}{m_i} \frac{1}{\omega_{ci}}. \end{aligned} \quad (2)$$

The indices i are relative to electrons and holes; m_i is the particle effective mass and ω the angular frequency; the relaxation time τ is infinite.

The important effect here is the presence in σ_{xx}^i of a nonlocal term which cannot be neglected: It is comparable in magnitude to the local term when the wave phase velocity is comparable to the carrier Fermi velocity as $q^2 R_i^2 = q^2 v_{Fi}^2 / \omega_{ci}^2$.

Under conditions (1), the Hall current vanishes if the plasma is compensated, and the dispersion equation reads

$$q^2 = i\mu_0 \omega (\sigma_{xx}^e + \sigma_{xx}^h), \quad (3)$$

where e and h refer to electrons and holes, and μ_0 is the vacuum permittivity. One obtains

$$q^2 \left(1 + \frac{2}{5} \frac{\sum_i n_i \epsilon_{Fi}}{B^2 / 2\mu_0} \right) = \omega^2 \mu_0 \frac{\sum_i n_i m_i}{B^2}. \quad (4)$$

Since $\frac{2}{5} n \epsilon_F$ is the kinetic pressure P_c of a Fermi gas, then Eq. (4) simplifies to

$$q^2 (1 + P_c / P_m) = \omega^2 (\mu_0 \rho / B^2), \quad (5)$$

where P_c , P_m are, respectively, the kinetic and magnetic pressure and ρ the mass density $\sum_i n_i m_i$. In terms of phase velocity, (5) reads

$$V_\phi = (v_A^2 + v_s^2)^{1/2}, \quad (6)$$

where v_A and v_s are the Alfvén- and the magneto-acoustic-mode phase velocities:

$$V_A = \left(\frac{B^2}{\mu_0 \rho} \right)^{1/2} = \left(\frac{2P_m}{\rho} \right)^{1/2}, \quad (7)$$

$$V_s = \left(\frac{2}{5} \frac{m_e v_{Fe}^2 + m_h v_{Fh}^2}{m_e + m_h} \right)^{1/2} = \left(\frac{2P_c}{\rho} \right)^{1/2}. \quad (8)$$

V_A is linear in B , V_s is independent of B .

Let us define B_{ac} , the acoustic coupling field,

i.e., the field for which the magnetic pressure is equal to the kinetic pressure, as

$$B_{ac}^2 = 2\mu_0 \rho_c. \quad (9)$$

Then

$$V_\phi = \left(\frac{B^2}{\mu_0 \rho} \right)^{1/2} \left(1 + \frac{B_{ac}^2}{B^2} \right)^{1/2}. \quad (10)$$

For high magnetic field, $B \gg B_{ac}$ and

$$V_\phi = V_A;$$

and for low magnetic field, $B \ll B_{ac}$ and

$$V_\phi = V_s.$$

Let us note that in the low-field limit $B \ll B_{ac}$, i.e., $P_c \gg P_m$, the dispersion equation (3) is equivalent from (5) to

$$\sigma_{xx}^e + \sigma_{xx}^h \simeq 0. \quad (11)$$

Therefore, the magnetoacoustic mode is a zero-current-density mode: The propagation mechanism is no longer of an electromagnetic nature. From this one concludes that, at a high magnetic field, an electromagnetic mode exists which, when the magnetic pressure is of the order of the kinetic pressure, couples with a mode which can be interpreted as an acoustic one. As discussed in Appendix A these modes are both compressional; their phase velocities are independent of frequency; the quantities $2P_m$ and $2P_c$ are the inverse of the magnetic and kinetic compressibilities of an electron-hole Fermi gas. As the magnetoacoustic mode consists of kinetic-pressure fluctuations, its phase velocity is of the order of the carrier's Fermi velocities.

B. Effects of Temporal Dispersion on Previous Theory

(i) Consider the case of the cyclotron-resonance regime ($\omega \sim \omega_{ci}$) under local conditions ($qR_i \sim 0$). As is well known,⁷ at a low magnetic field, the Alfvén wave couples with a longitudinal mode and propagation stops at the hybrid-resonance field B_h defined by

$$\omega = eB_h / (m_e m_h)^{1/2}.$$

The field B_h is between the electron- and hole-cyclotron-resonance fields. At B_h the two types of carriers oscillate in phase along the direction of propagation, i.e., $\sigma_{yy} = 0$. Since charge densities are screened at frequencies much lower than the plasma frequency, the current-density component j_y parallel to the wave vector is always zero, and the components E_y and E_x of the electric field are related by the equation

$$E_y = -(\sigma_{xy} / \sigma_{yy}) E_x.$$

Near the hybrid resonance, the mode is essentially longitudinal as $\sigma_{yy} \simeq 0$. The dispersion equation in

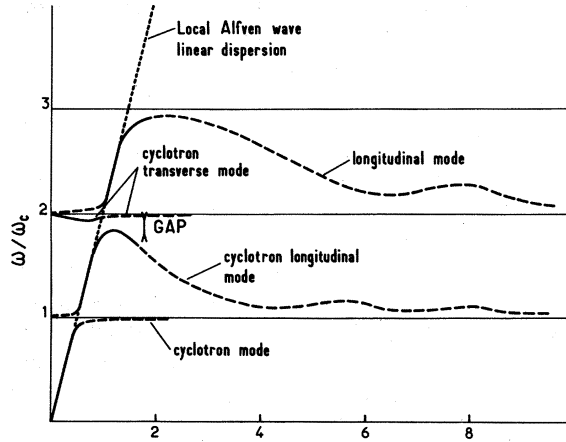


FIG. 1. Coupling of Alfvén waves to cyclotron waves in the vicinity of cyclotron resonances. Theoretical results: solid line, approximation up to $(qR)^2$ terms; broken line, calculation to higher terms.

the local limit ($qR_i \sim 0$) is easily derived from Eqs. (B7) and (C2), and the wave phase velocity is

$$V_\phi = V_A(1 - B_h^2/B^2)^{1/2}. \quad (12)$$

(ii) Taking into account the coupling with the magnetoacoustic mode ($qR_i \ll 1$), the phase velocity becomes

$$V_\phi = V_A(1 - B_h^2/B^2)^{1/2}(1 + B_{ac}^2/B^2)^{1/2}. \quad (13)$$

Therefore, at low magnetic fields, the Alfvén mode couples with the hybrid longitudinal mode and with the transverse magnetoacoustic mode. These effects have opposite results on the phase velocity. However, the hybrid-resonance field B_h varies linearly with frequency while the acoustic-coupling field does not; thus, experiments at low frequencies such that $B_h \ll B_{ac}$ would show the coupling of the Alfvén wave with the acoustic wave without any intervention of the longitudinal mode.

(iii) Let us now examine the validity of the theory leading to Eq. (13). We begin by restricting ourselves to the small spatial-dispersion regime of $qR_i \ll 1$. With the exception of the magnetoacoustic term, the other nonlocal terms in Eqs. (B7) need only be retained in a regime very close to cyclotron resonance. To be precise, let us suppose that the hole cyclotron resonance occurs at a much higher magnetic field than the electron cyclotron resonance, and that the coupling of the Alfvén wave to the magnetoacoustic wave is negligible. Under these conditions, at the hole-cyclotron-resonance field, there is no singularity in Alfvén-wave propagation in the local limit ($qR \sim 0$) because the rotation direction of the circularly polarized electromagnetic field is counter to the rotation direction of holes.⁷ Moreover, a theory^{8,9} taking into account all the nonlocal terms up to q^2R^2 shows that it is still true in a non-

local model. However, this nonlocal theory shows that the Alfvén wave near $\frac{1}{2}\omega_{ch}$ couples with a longitudinal cyclotron mode and with a transverse cyclotron mode. It also shows a surface impedance singularity near $\frac{1}{2}\omega_{ch}$ because at that point the group velocity cancels itself out. The main results of this theory⁸ are sketched in Fig. 1.

It goes without saying that, under strong nonlocal regime $qR_i > 1$, our theory of the coupling of the Alfvén mode with the magnetoacoustic mode does not apply. We note that the wave vector decreases with frequency. Then a lower experimental frequency allows us to restore the condition of small nonlocality ($qR_i < 1$) at a given magnetic field.

To summarize, the experimental study of the magnetoacoustic mode can be perturbed by the coupling of the Alfvén mode with the hybrid longitudinal mode, or with a cyclotron longitudinal mode, or by the occurrence of a strong nonlocal regime. In any case, work at sufficiently low frequencies should allow us to bypass these difficulties.

C. Theory for an Anisotropic Compensated Plasma-Bismuth

In the theoretical calculations, we use the ellipsoidal model for bismuth band energy; the hole ellipsoid is invariant by rotation around the trigonal axis ($\vec{3}$). The electron Fermi surface is composed of three ellipsoids slightly tilted out of the plane perpendicular to the ternary axis. The equation of ellipsoid (a), invariant by symmetry with respect to the binary axis ($\vec{1}$) reads, in the right triad ($\vec{1}, \vec{2}, \vec{3}$), where $\vec{2}$ is the bisectrix axis

$$2m_0\epsilon_{Fe} = \alpha p_1^2 + \beta p_2^2 + \gamma p_3^2 + \epsilon p_2 p_3. \quad (14)$$

Ellipsoids (b) and (c) are deduced from ellipsoid (a) by $\pm 120^\circ$ rotations around the ternary axis.

The hole ellipsoids equation is

$$2m_0\epsilon_{Fh} = a(p_1^2 + p_2^2) + bp_3^2. \quad (15)$$

The electron and hole inverse-mass tensors are deduced from the mass system obtained by Williams¹ from Alfvén-wave propagation experiments. The effective masses at the Fermi surface (in units of m_0) are as follows: For electrons, $m_1 = 0.005$, $m_2 = 1.27$, $m_3 = 0.031$, $m_4 = 0.157$; hence $\alpha = 200$, $\beta = 2.106$, $\gamma = 86.28$, $\epsilon = -10.67$. For holes, $M_1 = 0.064$, $M_2 = 0.064$, $M_3 = 0.69$; hence $a = 15.62$, $b = 1.45$. The sign of m_4 is positive in the right triad ($\vec{1}, \vec{2}, \vec{3}$), identical with the ($\vec{1}^*, \vec{2}^*, \vec{3}^*$) triad defined by Brown, Hartman, and Koenig.¹⁰ Following Smith, Baraff, and Rowell,¹¹ we use for the electrons Fermi energy ϵ_{Fe} , hole Fermi energy ϵ_{Fh} , band overlap energy ϵ_0 , and carriers density n the following values: $\epsilon_{Fe} = 27.6$ meV, $\epsilon_{Fh} = 10.9$ meV, $\epsilon_0 = 38.5$ meV, $n = 2.75 \times 10^{23}$ m⁻³. The band overlap energy is given by $\epsilon_0 = \epsilon_{Fe} + \epsilon_{Fh}$ as shown in Fig. 2. From these quantities, one deduces that the acoustic-coupling field value B_{ac} must be 400 G

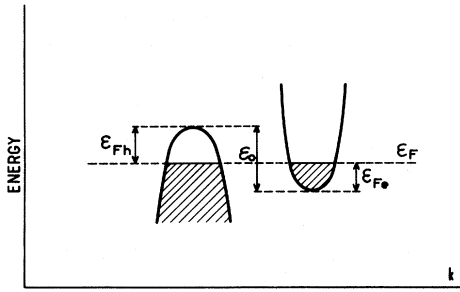


FIG. 2. Schematic main energy bands of bismuth showing the overlap.

for the magnetic pressure to be equal to the kinetic pressure.

We can now discuss qualitatively the case of bismuth. As shown in the isotropic model, the coupling of the Alfvén mode with the magnetoacoustic mode can be observed clearly if the coupling with the longitudinal hybrid mode and the longitudinal cyclotron mode occurs for magnetic fields smaller than the acoustic-coupling field.

In Fig. 3 we have plotted, depending on the orientation of the magnetic field in a plane perpendicular to the binary, bisectrix, and trigonal respectively, the variation of the cyclotron- and hybrid-resonance fields for the two experimental frequen-

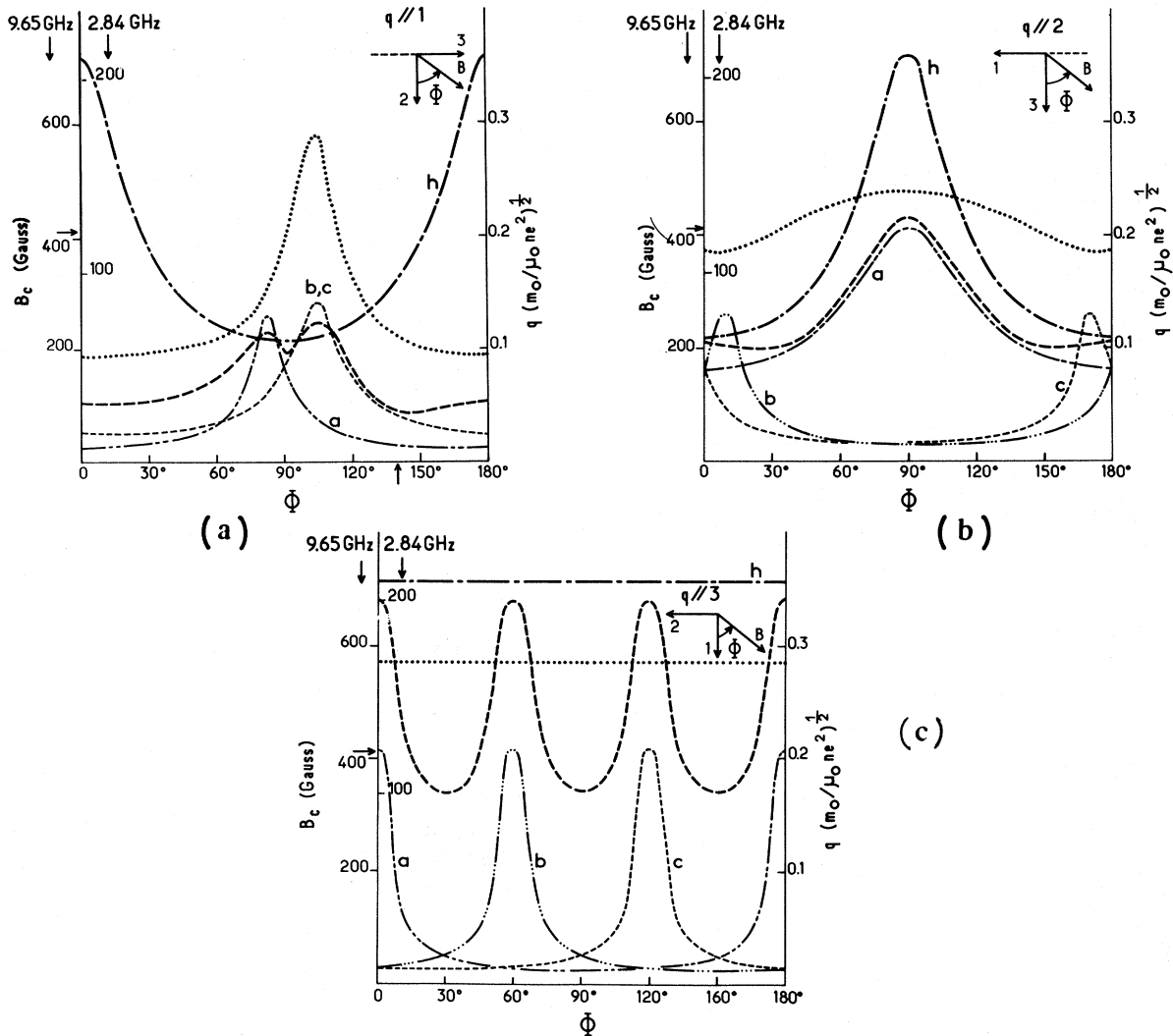


FIG. 3. Anisotropy of cyclotron-resonance and hybrid-resonance fields for two experimental frequencies. (a) \vec{q} is parallel to 1 axis; (b) \vec{q} is parallel to 2 axis; (c) \vec{q} is parallel to 3 axis. Cyclotron-resonance fields versus direction of \vec{B} for each type of carriers: ---- electrons a ; - · · · - electrons b ; - - - electrons c ; - - - holes; ---- hybrid-resonance field versus direction of \vec{B} . The arrow on the B_c scale points out the B_{ac} field. . . . curve showing in dimensionless units $q(m_0/\mu_0 n e^2)^{1/2}$ the wave vector of compressional Alfvén wave at 9.65-GHz frequency and 10-kg magnetic field versus direction of \vec{B} .

The figure shows two diagrams, I and II, representing different orientations of a carrier relative to a magnetic field B (indicated by a circle with a dot). Diagram I shows the carrier along the large principal axis, and Diagram II shows it along a small principal axis. Below the diagrams is a table with two columns for 'Small' and 'large' magnitudes.

$mc \propto (p_x p_y)^{1/2}$	Small	large
$\sigma_{xx} \propto (p_y)^2$	Small	Small
$R_y \propto p_x$	Small	large
$\sigma_{yy} \propto (p_x)^2$	Small	large
$R_x \propto p_y$	Small	Small

FIG. 4. Table showing relative magnitude of cyclotron masses, transverse conductivities, and spatial exploration-radius components.

cies 2.84 and 9.65 GHz. At 2.84 GHz, the hybrid- and cyclotron-resonance fields are much smaller than the acoustic-coupling field for all orientations. At 9.65 GHz, this takes place when the direction of propagation is parallel to the binary axis [Fig. 3(a)]. But the contrary happens when the magnetic field is along the binary axis [Figs. 3(b) and 3(c)]. The condition $qR_i \ll 1$ is less simple to discuss. Let us note, however, that an orientation for which all cyclotron masses are small corresponds to long-wavelength propagation and to small spatial dispersion, so that the condition of small spatial dispersion is also more easily fulfilled. This can be easily understood if one takes the crude model of a cigar-shaped ellipsoidal Fermi surface; the results are shown in Fig. 4. We have indicated the relative magnitude of cyclotron masses, transverse conductivities, and spatial exploration radii for the two following situations: the magnetic field along the large principal axis (I) and along a small principal axis (II). It follows that, when the cyclotron mass is small, the carrier is frozen in the plane transverse to the magnetic field: The transverse conductivity and the spatial exploration are both small. This carrier only contributes to the Hall current. Thus, in the base of bismuth, when all cyclotron masses are small, the Alfvén conductivity, and therefore the wave vector \vec{q} , and the spatial exploration radius R_i are small, so that the nonlocal parameters qR_i are small.

In Fig. 3, we have also plotted the Alfvén wave vector at frequency 9.65 GHz, and for a magnetic field of 10 kG. It can be verified that when cyclotron masses are small the wave vector is also small.

We now develop the general theory for bismuth. Since the electrons and holes Fermi surface in bismuth are ellipsoidal to a good approximation, one first needs to know the general nonlocal conductivity tensor for an ellipsoidal Fermi surface. This ten-

sor $\vec{\sigma}^E$ can be derived from the conductivity tensor for a spherical surface $\vec{\sigma}^S$ by mathematical transformations, but we prefer to derive it through simple physical arguments. This is done in Appendix B.

In the general case, one has to solve the complete dispersion equation (cf. Appendix C). We calculate the conductivity tensor by summing up the contributions of each ellipsoid. This calculation is done in the region of small spatial dispersion ($qR_i \ll 1$). We just keep the magnetoacoustic term and neglect the other nonlocal terms, i. e., we do not take into account the coupling with the cyclotron longitudinal mode; the temporal hybrid-resonance effect is included. In fact, one should remark that the coupling of the Alfvén mode with the cyclotron longitudinal mode is only noticeable in the cyclotron-resonance region $\omega_{ci} \sim \omega$. On the other hand, the coupling with the hybrid longitudinal mode and transverse magnetoacoustic mode begins for fields greater than B_h or B_{ac} , as is obvious from Eq. (13). In this approximation, the dispersion equation is quadratic in q^2 , and thus can be solved algebraically. The calculations are long but straightforward. They have been processed on an IBM 1130 computer. The validity of the small spatial-dispersion approximation ($qR_i < 1$) is checked *a posteriori*.

We will now show an interesting result: In a case where the Alfvén wave couples only with the magnetoacoustic mode, the study of the coupling of these two modes can yield, in principle, the quantity $n\epsilon_0$.

Let us assume that the two modes, solutions of the dispersion equation, are electrically polarized parallel and transverse, respectively, to the magnetic field. This assumption is well verified for a high-symmetry direction or in a high-magnetic-field regime (cf. Appendix C). The dispersion equation is

$$q^2 = i\mu_0\omega(\sigma_{xx}^E - \sigma_{xy}^E/\sigma_{yy}^E). \quad (16)$$

(The Hall term σ_{xy}^E is different from zero in the high-field limit because of the anisotropy of bismuth, and is of the order of $1/B^2$.) As shown in Appendix B, the magnetoacoustic term in σ_{xx}^E , called $\sigma_{xx}^{E nl}$, is isotropic. (The superscript nl stands for nonlocal.) This is physically clear if one realizes that this term represents the kinetic-pressure contribution to the transverse conductivity σ_{xx}^E .

Equations (16) and (B22) then yield

$$q = \frac{q_{loc}}{(1 + P_c/P_m)^{1/2}}, \quad (17)$$

where q_{loc} , the dispersion-equation solution in the local approximation, is linear in $1/B$.

Since the three electron ellipsoids of bismuth have the same Fermi energy ϵ_{Fe} , the total electron contribution to the kinetic pressure P_c is equal to $\frac{2}{5}n\epsilon_{Fe}$, so that the total kinetic pressure is

$$P_c = \frac{2}{5} n (\epsilon_{Fe} + \epsilon_{Fh}) . \quad (18)$$

As shown in Fig. 2, the quantity $\epsilon_{Fe} + \epsilon_{Fh}$ is just the band-energy overlap ϵ_0 , so that

$$P_c = \frac{2}{5} n \epsilon_0 . \quad (19)$$

Thus, the study of the deviation of the dispersion law from a linear law in $1/B$ can yield the quantity $n\epsilon_0$.

We can now discuss the possibility of observing the coupling of the compressional Alfvén mode with the magnetoacoustic mode in solid-state compensated plasmas. In compensated metals, the carriers' density is so high that the kinetic pressure is always much higher than the magnetic pressure in laboratory magnetic fields. Thus, for magnetic fields such as

$$B_h \ll B \ll B_{ac} , \quad (20)$$

one can excite, in principle, a very pure acoustic mode completely decoupled from the Alfvén wave. In that case, as shown previously, the acoustic mode is an almost perfect zero-current mode and will be very difficult to excite. In bismuth, on the contrary, the carriers' density is much lower than in metals, so that the kinetic pressure, hence B_{ac} , is rather low. Thus, the problem in bismuth is to work at sufficiently low frequencies, such as

$$B_{ct}, B_h \ll B_{ac} \sim B, qR_t \ll 1 , \quad (21)$$

where the cyclotron-resonance field B_{ct} is defined by

$$\omega = eB_{ct}/m_t .$$

But in a solid-state plasma, since the momentum relaxes essentially to the lattice, the frequency has to be sufficiently high such that

$$\omega\tau \gg 1 .$$

Even for the best bismuth samples, at pumped liquid-helium temperature, these two conditions define a rather narrow window of frequencies from $\nu = 2$ GHz ($\omega\tau \sim 10$) to $\nu = 10$ GHz ($B_h \sim B_{ac}$).

III. EXPERIMENTAL METHOD

A. Sample Preparation

Single-crystal ingots are grown from a melt of 99.9999 bismuth by a modified Kapitza's method in a hydrogen atmosphere. In a horizontal boat submitted to a temperature gradient, crystallization starts from a single crystal germ. After crystallographic orientation using x rays, flat disks are cut with a spark machine from the ingots. They are mechanically lapped; the strained parts are removed by chemical etching and electrolytic polishing. Finally the samples are annealed at 250 °C during 100 h in hydrogen flow; our samples have an average collision time of about 3×10^{-10} sec.

B. X-Band Methods

We use a transmission method with a sample placed between two tuned cavities; this method was originally used for paramagnetic spin-resonance experiments.¹²

The cavities are parallelepipedic, iris coupled to the waveguides. One of them is frequency tunable by means of a Teflon plunger. The signal coming from the reception cavity is sent on a hot-electron InSb bolometer, put in the low-temperature cryostat where the experiment is performed. The magnetic field is modulated at a very low frequency (12 Hz). A microwave reference signal with adjustable amplitude and phase is applied also to the InSb detector. The output signal from the bolometer is sent to a lock-in amplifier.

The static magnetic field is applied parallel to the plane face of the sample. Figure 5 shows a simplified scheme of the cavities, detector, and coaxial cable for the reference signal.

C. 10-cm-Band Methods

The setup of an experiment similar to the X-band experiment should induce heavy experimental difficulties related to the dimensions of parallelepipedic cavities with a wavelength of the order of 10 cm.

A one-dimensional resonant structure is much more compact, therefore we conceived an experimental setup using two "strip" cavities tuned at the

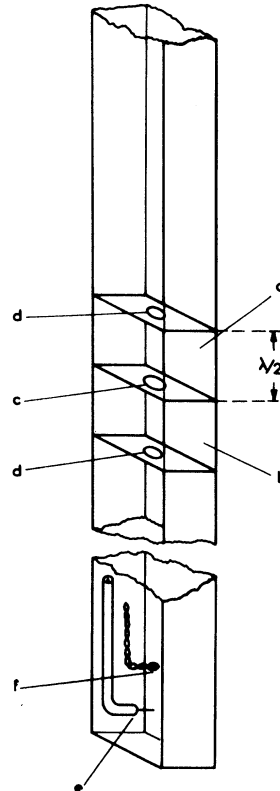


FIG. 5. Schematic experimental setup for the 3-cm-band frequencies. (a): emission cavity; (b): reception cavity; (c): sample; (d): coupling iris; (e): antenna for the reference signal; (f): InSb hot-electron bolometer.

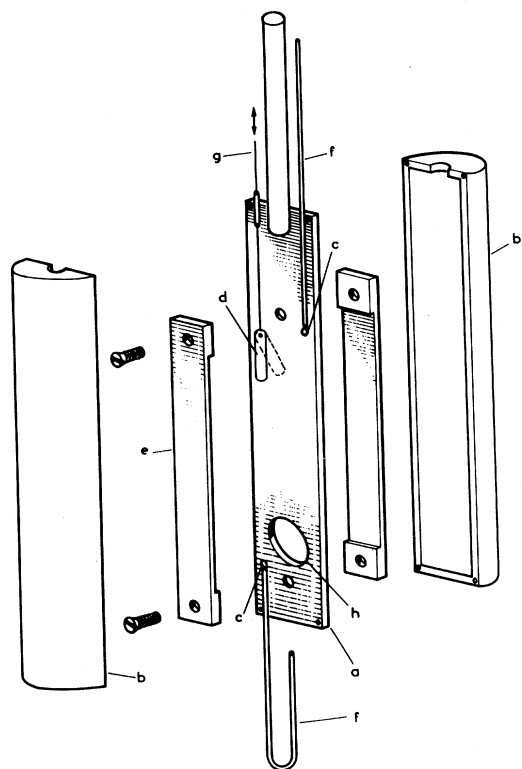


FIG. 6. Exploded view of the 10-cm-band setup. (a): ground base plate; (b): brass covers; (c): coupling loops; (d): Teflon plunger for frequency adjustment; (e): strip resonators; (f): coaxial cables; (g): pusher actuating the Teflon plunger; (h): sample position. For clarity the coupling loops of the second cavity and the sample diaphragms are not shown.

same frequency and coupled by transmission through the sample. Such a setup has very acceptable dimensions.

Each cavity is made of a section of a nonbalanced copper strip line (width 10 mm, dielectric thickness 1 mm, length $\frac{1}{2}\lambda$) short-circuited at both ends. The dielectric is liquid helium during the experiment. Excitation of the cavities is done magnetically: A small loop ($\phi = 1$ mm) put at the end of the semirigid coaxial cable is pressed laterally against the strip line in the neighborhood of a short-circuited end. (In such a point there is a node of electric field and a maximum of magnetic field.) The coupling is adjusted by changing the position of the loop with respect to the end of the strip line and its orientation around the axis of the coaxial cable. The ground base plate common to each cavity is used as sample holder; for this purpose a circular hole of a slightly greater diameter than the sample diameter is drilled into the plate. The plate has the thickness of the sample. The hole is near the short-circuited ends of the two cavities. The sample is fixed inside

with silver glue. Two annular diaphragms made of fine gold (0.15 mm thick, external diameter 15 mm, internal diameter 4 mm), fixed also with silver glue, cover each face of the sample. They have a double role: to suppress the microwave leakage between the two cavities, and also to limit the effective surface of the sample in order to get rid of surface-impedance variation with the magnetic field, which would modify the Q of the cavities.

The characteristic impedance of the strip line is 30Ω *in vacuo*. This value, smaller than the vacuum impedance, limits diffraction losses. The cavities are electrically isolated by two semicylindrical brass covers the internal faces of which are painted with a microwave absorbant colloidal graphite to avoid parasitic resonance modes. Indium gaskets ensure a better than 100-dB isolation between the cavities.

Each cavity has two magnetic-coupling loops with a maximum distance between them. By using one loop for the emission and one for the reception, one can separately measure the resonance frequency f_c and the quality factor Q of each cavity. During the transmission experiment only one loop is used with each cavity: one for the emission, the other for the reception.

A small piece of Teflon, articulate on an axis fixed on the ground base plate, furnishes a means of tuning the cavities. This system gives a variation of f_c of the order of 30 MHz.

The quality factor of the cavities was measured by transmission. At critical coupling, $Q \approx 500$ (therefore the intrinsic¹³ quality factor $Q_0 \approx 1500$).

Figure 6 shows the described system. The coupling loops have been drawn for one cavity only. The magnetic field \vec{B} is parallel to the sample.

A detection setup for the transmitted signal in the 3-GHz band is shown in Fig. 7; the microwave with frequency Ω is amplitude modulated at frequency ω (typically 700 Hz) by a diode modulator.

A stub stretcher tunes the source to the first-cavity excitation loop. Another stub stretcher

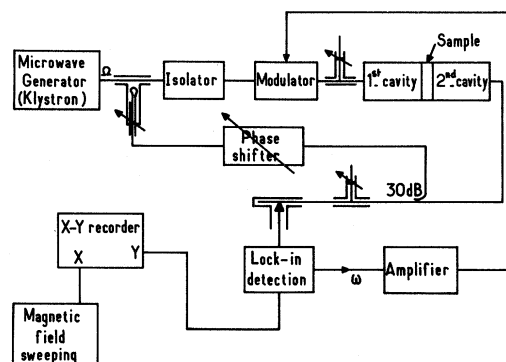


FIG. 7. $3Gc/v$ detection setup.

adapts the second-cavity loop to a detection diode fitted up on the coaxial line.

A small part of the nonmodulated signal can be sampled at the output of the generator by an adjustable attenuation coupler followed by a phase shifter, and sent onto the detection diode by means of a directional coupler, so as not to perturb the reception cavity. The signal at frequency ω from the diode is sent on a lock-in detector. We thus have a homodyne system where a reference signal interferes with the transmitted one; one observes transmission extrema when

$$\frac{1}{2}p\lambda = d,$$

where d is the sample thickness, λ the wavelength in the medium, and p an integer.

IV. EXPERIMENTAL RESULTS AND COMPARISON WITH THEORY

The main experimental results are presented in the following figures. We have plotted there the number of half-wavelengths in the sample, proportional to the wave vector, as a function of the inverse of the magnetic field. The following theoretical results are also presented: the local dispersion curve taking account of the coupling with the hybrid longitudinal mode; the curve, linear in $1/B$, asymptotic in the high-field limit to the local dispersion curve; and the nonlocal dispersion curve including the coupling with the magnetoacoustic mode. The deviation of the local curve from the asymptotic one allows us to appreciate the importance of the coupling with the hybrid longitudinal mode, the deviation of the nonlocal curve from the local one, and the importance of the coupling with the magnetoacoustic mode. We also plot for each ellipsoid the nonlocal parameter qR_i ; this allows us to verify *a posteriori* the validity of the power-series expansion to the order $(qR)^2$. The fit between the experimental plot and nonlocal theory has been done for one point ($B = 2000$ G).

A. Coupling with the Magnetoacoustic Mode

A very spectacular and characteristic example of Alfvén- and magnetoacoustic-wave coupling is presented in Fig. 8(a). In the high-magnetic-field limit, the wave vector displays a linear dependence on $1/B$, typical of Alfvén-wave dispersion; in the low-field limit, it tends to a constant value characteristic of the magnetoacoustic wave.

The particularity of this special orientation of \vec{B} and \vec{q} , is twofold: First the hybrid- and cyclotron-resonance fields are much smaller than the acoustic-coupling field [Fig. 3(a)], and therefore do not affect the magnetoacoustic interaction. Also, in this orientation the cyclotron masses are small and the condition of small spatial dispersion is satis-

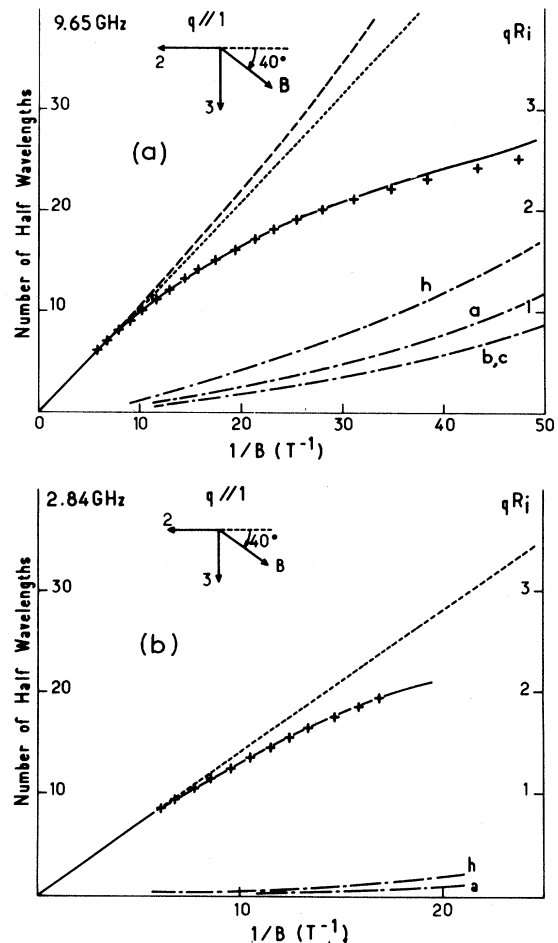


FIG. 8. Dispersion law versus $1/B$ in the direction $\vec{q} \parallel \vec{I}$ with $(\vec{q}, \vec{B}) = 140^\circ$. (a) Propagation at 9.65 GHz, $T = 1.8^\circ\text{K}$, sample thickness 0.25 mm; (b) propagation at 2.84 GHz, $T = 1.8^\circ\text{K}$, sample thickness 1.36 mm. At this frequency, in the range of magnetic field, the local dispersion curve and its high-field asymptote become superimposed. Theoretical curves: — — — local dispersion curve including hybrid-resonance effect; - - - linear versus $1/B$ curve asymptotic at high fields to the local dispersion curve; — — — dispersion curve including the nonlocal magnetoacoustic and the hybrid-resonance effect; — - — curves of qR_i for the different ellipsoids of carriers electrons a , b , c and holes h ; + experimental points.

fied. These two points are confirmed by the general agreement with theory; there is however a small disagreement at very low field, probably due to a rather large-hole nonlocal parameter, as shown in the figure. The deviation of the local theoretical curve from the asymptotic linear curve shows, as discussed at the end of Sec. II C, that the coupling with the hybrid longitudinal mode is noticeable even at fields high compared to the hybrid-resonance field. Therefore, the study of the coupling of the Alfvén and magnetoacoustic waves for that particu-

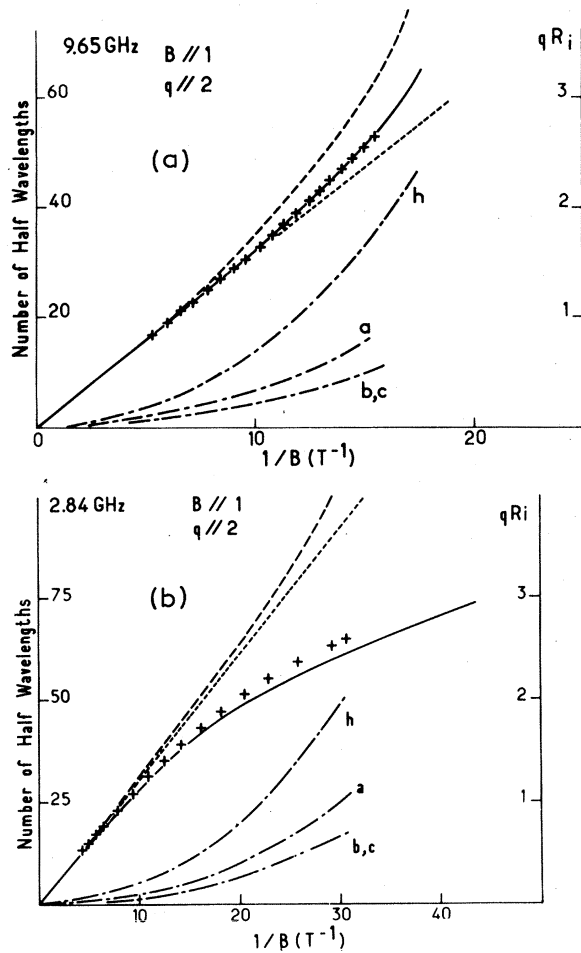


FIG. 9. Same as Fig. 8. (a) Propagation at 9.65 GHz with $\vec{B} \parallel \vec{1}$ in the direction $\vec{q} \parallel \vec{2}$; $T = 1.8^\circ\text{K}$; sample thickness 0.42 mm. (b) Propagation at 2.84 GHz with $\vec{B} \parallel \vec{1}$ in the direction $\vec{q} \parallel \vec{2}$. $T = 1.8^\circ\text{K}$; sample thickness 1.34 mm.

lar frequency cannot precisely yield the quantity $n\epsilon_0$.

However, at lower frequency, the coupling with the hybrid longitudinal mode should be smaller. Experimental result for a lower frequency is thus presented in Fig. 8(b). One observes the characteristic coupling with a magnetoacoustic mode, and according to theory the coupling with hybrid longitudinal mode is negligible in the considered range of field. However, we observe wave propagation only down to 500 G, owing to a lower $\omega\tau$. The derivation of the quantity $n\epsilon_0$ will be discussed in Sec. IV E.

B. Influence of Coupling with the Hybrid Longitudinal Mode

We show in Figs. 9 and 10 how the hybrid longitudinal mode can affect the magnetoacoustic coupling. At 9.65 GHz [Fig. 9(a)], the experimental

dispersion law is controlled by the approach to hybrid resonance; at 2.84 GHz, on the other hand, the hybrid resonance is pushed down to low fields and the magnetoacoustic coupling appears clearly.

Let us be more explicit. This hybrid resonance is due to the oscillation in phase along the direction of propagation of electrons a and holes. At high frequency and for this orientation the hybrid-resonance field can be obtained from Fig. 3(b): $B_h = 370$ G. The theoretical analysis of the experimental dispersion curve shows that the coupling with the magnetoacoustic mode is only slightly smaller than the coupling with the hybrid longitudinal mode; this appears clearly in the dispersion curves of Fig. 9(a). By comparing the two theoretical dispersion curves, the importance of the hidden magnetoacoustic coupling can be appreciated. Thus, the excellent fit of theory and experiment represents an indirect confirmation of the magnetoacoustic effect. Let us remark that the agreement is good even at low fields where the hole nonlocal parameter is rather large. This can be explained by

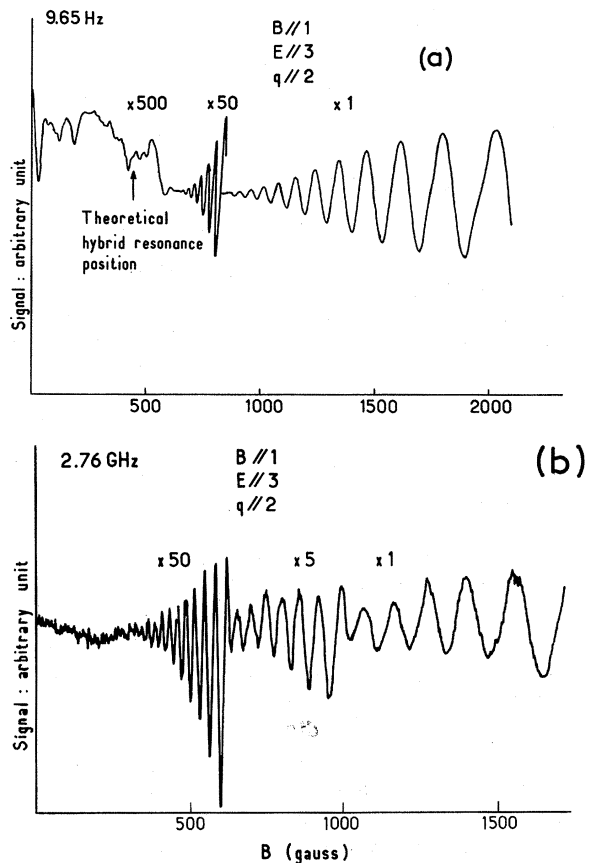


FIG. 10. (a) Experimental recording at frequency 9.65 GHz; $T = 1.8^\circ\text{K}$; sample thickness = 0.40 mm. (b) Experimental recording at frequency 2.76 GHz; $T = 1.8^\circ\text{K}$; sample thickness = 1.34 mm.

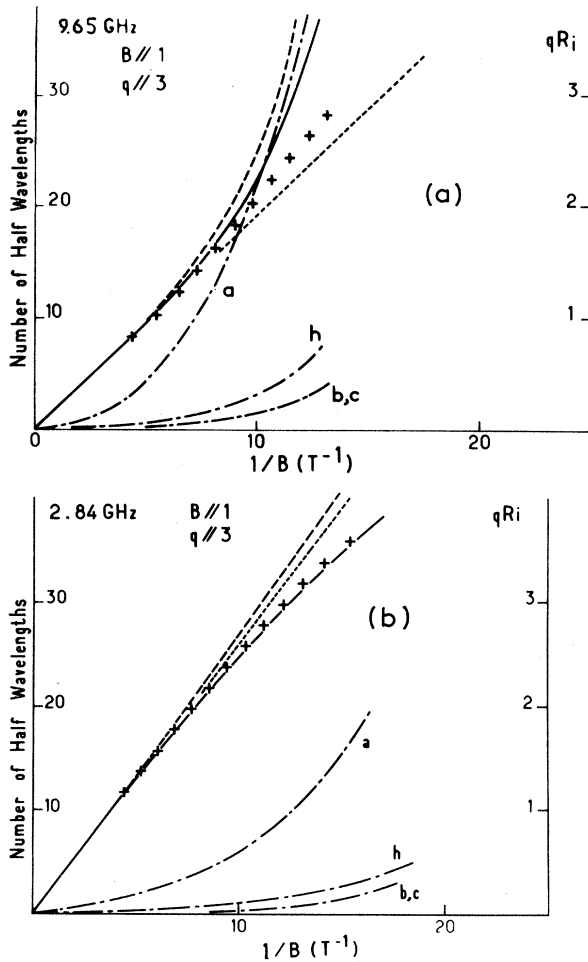


FIG. 11. Same as Fig. 8: (a) Propagation at 9.65 GHz with $\vec{B} \parallel \vec{I}$ in the direction $\vec{q} \parallel \vec{z}$; $T = 1.8^\circ\text{K}$; sample thickness 0.17 mm. (b) Propagation at 2.84 GHz with $\vec{B} \parallel \vec{I}$ in the direction $\vec{q} \parallel \vec{z}$; $T = 1.8^\circ\text{K}$; sample thickness 0.94 mm.

a small hole contribution to the Alfvén current in that orientation.

Figure 9(b), by comparison with Fig. 9(a), shows that at lower frequencies, the coupling with the hybrid longitudinal mode, for a given magnetic field, is much smaller. In fact, one observes a very strong coupling to the magnetoacoustic mode, and one can follow the wave propagation down to fields twice as small as for the higher frequency. There is, however, a slight disagreement with theory at low magnetic field. We do not have any explanation for it. (For this sample, frequency, and orientation, we have $\omega\tau \sim 9$, so that the effect of the finiteness of $\omega\tau$ should still be rather small.)

In Fig. 10 we present the experimental recordings for both frequencies. In Fig. 10(a), one observes between the theoretical hybrid-resonance field and the onset of wave propagation, a surface-impedance

singularity which is not explained by the present theory.

C. Influence of Strong Spatial-Dispersion Regime

In Fig. 11(a) an interesting example of combined hybrid resonance and large spatial-exploration effect is presented. The experimental dispersion curve shows the qualitative feature of the coupling with a longitudinal hybrid mode, due to electrons a and holes. This fits poorly with theory owing to the large nonlocal parameter of electrons a . The experimental coupling with the hybrid mode for a given magnetic field is much smaller than what is predicted by the small spatial-dispersion theory. We propose the following explanation: The conductivity of electrons a is decreased owing to their high nonlocal parameter and therefore the hybrid resonance is shifted to lower magnetic fields (i.e., towards the electrons- a cyclotron field). The nonlocal effect on the dispersion curve is magnified by the vi-

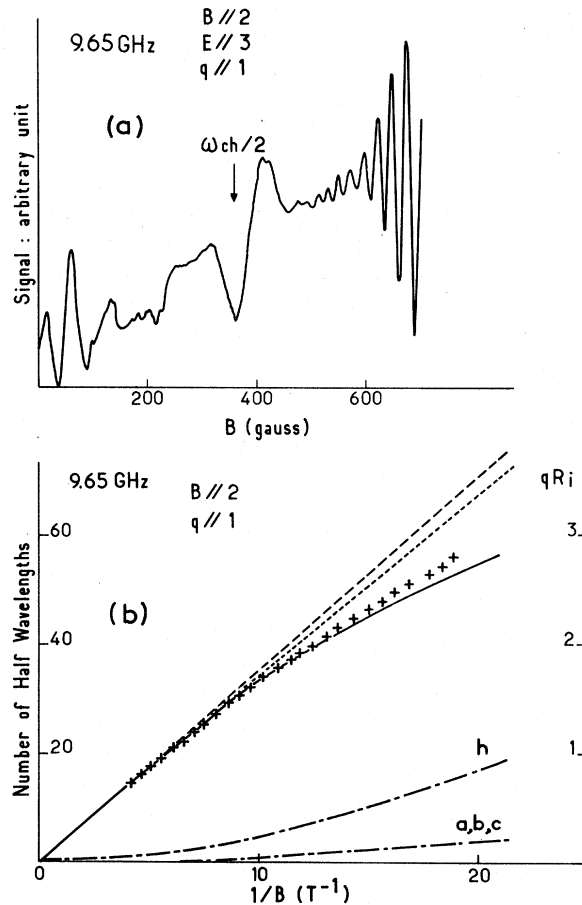


FIG. 12. (a) Experimental recording at frequency 9.65 GHz with $\vec{B} \parallel \vec{z}$ in the direction $\vec{q} \parallel \vec{I}$; $T = 1.8^\circ\text{K}$; sample thickness 1.36 mm. (b) Same as Fig. 8 for propagation at 9.65 GHz with $\vec{B} \parallel \vec{z}$ in the direction $\vec{q} \parallel \vec{I}$; $T = 1.8^\circ\text{K}$; sample thickness 1.36 mm.

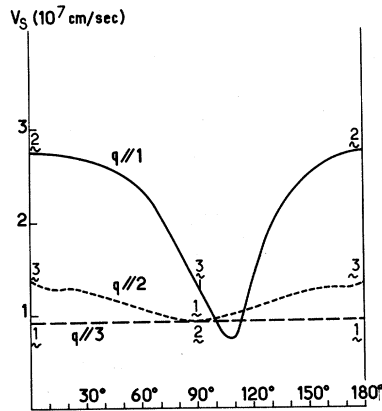


FIG. 13. Magnetoacoustic-mode phase velocity versus direction of magnetic field: — for $\vec{q} \parallel \vec{1}$ (\vec{B} direction varies from 2 axis to 3 axis); --- for $\vec{q} \parallel \vec{2}$ (\vec{B} direction varies from 3 axis to 1 axis); - · - for $\vec{q} \parallel \vec{3}$ (\vec{B} direction varies from 1 axis to 2 axis).

cinity of a hybrid resonance ($\sigma_{yy} \sim 0$). For that particular orientation and frequency, the hybrid-resonance field B_h (calculated in the local limit) is much higher than the magnetoacoustic field B_{ac} ; therefore, the coupling with the magnetoacoustic mode is negligible.

On the other hand, an experiment at lower frequency, presented in Fig. 11(b), allows us to observe clearly the coupling with the magnetoacoustic mode; the coupling with the hybrid longitudinal mode, although not negligible, is strongly reduced; the agreement with theory is quite good. The important nonlocality ($qR > 1$) of electrons a at low magnetic field, even for that low frequency, has no observable effect, because for this geometry electrons a have a small contribution to the Alfvén conductivity.

D. Influence of Coupling with a Cyclotron Longitudinal Mode

An interesting experimental recording is presented in Fig. 12(a): One observes wave propagation from high magnetic field down to a surface-impedance singularity. For that orientation, the cyclotron masses of electrons a , b , c are much smaller than for holes. Then the hybrid-resonance field is lower than the hole subharmonic cyclotron-resonance field $\frac{1}{2}\omega_{ch}$ [cf. Fig. 3(a)]. Thus the theoretical model of the coupling of the Alfvén wave with the cyclotron longitudinal mode applies. The hole fundamental cyclotron resonance is not observed. As predicted by theory, a strong surface-impedance singularity is observed near $\frac{1}{2}\omega_{ch}$. The experimental dispersion curve is presented in Fig. 12(b). From the high-field side down, one first observes the coupling with the magnetoacoustic mode. Then the experimental dispersion curve deviates from

the theoretical nonlocal curve. We interpret this disagreement by the coupling with the cyclotron longitudinal mode near $\frac{1}{2}\omega_{ch}$ ^{9,14,15} which we have not taken into account in the theory developed in this paper.

E. Experimental Determination of $n\epsilon_0$

All experiments at 2.84 GHz present a clear evidence of the compressional Alfvén-mode coupling with the magnetoacoustic mode. In all geometries, theory and experiment fit well together. In most orientations, the coupling with the hybrid longitudinal mode may be inferred by theory to be negligible in the experimental magnetic field range of wave propagation. The analysis of the deviation of the dispersion curve from the asymptotic one allows us to determine experimentally the product of the carriers' density by the band overlap energy:

$$n\epsilon_0 = 1550 \pm 160 \text{ J m}^{-3}.$$

This value is consistent with the value of $n\epsilon_0$ (1680 J m^{-3}) derived from Smith, Baraff, and Rowell.¹¹

In conclusion, we present in Fig. 13 the phase velocity of the magnetoacoustic mode for different orientations. It is interesting to point out that, as is clear from Eq. (8), the phase velocity of this mode presents the same anisotropy as the Alfvén-mode phase velocity in the high-field local limit.

V. CONCLUSION

The main results obtained in this paper are the following:

(i) At 2.8 GHz a very clear coupling of the Alfvén wave with the magnetoacoustic mode is observed in bismuth, for all directions; at this frequency the effects of hybrid or cyclotron resonance and non-local terms are negligible.

(ii) At 10 GHz in the direction of very small cyclotron masses, $(\vec{2}, \vec{B}) = 140^\circ$, $\vec{q} \parallel \vec{1}$, the coupling is clearly observed; for all other directions we have taken into account the presence of hybrid cyclotron-resonance and nonlocal phenomena in order to get a good agreement between theory and experiments.

(iii) Finally, a value of $n\epsilon_0$ has been deduced from these experiments.

One would like to emphasize the very good agreement between theory and experiment in all this work.

We have not studied here the electron-hole acoustic mode in the absence of a magnetic field. It is a purely longitudinal excitation which does not couple with a transverse electromagnetic probe; this difficulty has been clearly analyzed by McWhorter and May.³ The best way to study this mode, although still very difficult, may be a light-scattering experiment, as suggested by Wolff.¹⁶

APPENDIX A

We present in this appendix a discussion of the physical nature of the Alfvén and magnetoacoustic modes from two distinct points of view, first from the magnetohydrodynamic theory, then from the electromagnetic one.

The physical concepts relevant to the propagation of magnetohydrodynamic waves in conducting fluid are given by Alfvén and Falthammer.¹⁷ We briefly recall Alfvén's magnetohydrodynamic theory, and show how it applies even in the case of a collisionless compensated plasma.

In the low-frequency and long-wavelength range, the magnetohydrodynamic theory applies. The local thermodynamic equilibrium is achieved under the following conditions:

$$\begin{aligned} \omega\tau &\ll 1, \\ q\langle v \rangle\tau &\ll 1, \end{aligned} \quad (\text{A1})$$

where τ is a characteristic collision time of the conducting fluid, $\langle v \rangle\tau$ the mean free path, and ω and \vec{q} the frequency and wave vector of the described phenomena.

In the presence of a magnetic field the situation is complex: When a conducting fluid element moves in a magnetic field, an induced electric field appears, hence also an electric current density \vec{j} that modifies the magnetic field distribution and a magnetic force $\vec{j} \times \vec{B}$ on the fluid element concerned.

Nevertheless, an elegant and simple model can explain the magnetohydrodynamic propagation phenomena if one considers the following physical facts (Ref. 17, p. 83):

(a) For a high-conductivity fluid, the magnetic field lines are "frozen", i. e., the magnetic field flux through any contour of moving and deforming conducting matter is constant. The inertia of conducting matter can then be ascribed to the force tubes containing it.

(b) The force $\vec{j} \times \vec{B}$ exerted by the magnetic field \vec{B} on the fluid element with current density \vec{j} is equivalent to a tension $B^2/2\mu_0$ and a transverse pressure $B^2/2\mu_0$.

(c) The fluid has an adiabatic compressibility

$$\chi_c = 1/\gamma P_c, \quad (\text{A2})$$

where P_c is the kinetic pressure of the fluid and γ the ratio C_p/C_v . For a system with l degrees of freedom,

$$\gamma = (2+l)/l. \quad (\text{A3})$$

In the magnetohydrodynamic limit, we have three degrees of freedom, so $\gamma = \frac{5}{3}$.¹⁸ Therefore, for a wave propagating perpendicular to the static magnetic field, a fluid element moving along the direction of propagation is submitted to magnetic and

kinetic pressure fluctuations. The phase velocity then is

$$v_\phi = (1/\rho\chi)^{1/2}, \quad (\text{A4})$$

where ρ is the volumic mass and χ the compressibility given by

$$\chi^{-1} = \chi_c^{-1} + \chi_m^{-1}. \quad (\text{A5})$$

The magnetic compressibility is derived from the magnetic pressure P_m :

$$P_m = B^2/2\mu_0, \quad \chi_m = 1/2P_m. \quad (\text{A6})$$

Thus, the phase velocity is easily expressed as

$$v_\phi = (v_s^2 + v_A^2)^{1/2}, \quad (\text{A7})$$

where

$$v_s = (\frac{5}{3} P_c / \rho)^{1/2}, \quad v_A = (2P_m / \rho)^{1/2}. \quad (\text{A8})$$

v_A is the Alfvén velocity, linear in B . At a magnetic field large enough for the magnetic pressure to be greater than the kinetic pressure, the wave just described corresponds to the compressional Alfvén wave, and at low magnetic field it yields the acoustical mode.

We now consider a collisionless plasma; the mean free path is large compared to all other characteristic physical dimensions. We assume that the following inequalities are verified:

$$\omega\tau \gg 1, \quad (\text{A9})$$

$$q\langle v \rangle\tau \gg 1.$$

Such a plasma can exist in gas discharge and some astrophysical problems, but also in a solid-state plasma, such as bismuth.

A hydrodynamic description of the problem in terms of pressure, density, and velocity of a fluid element does not seem possible as there is no collision mechanism to randomize the velocity distribution. Nevertheless, as suggested by Alfvén and Falthammer¹⁷ and Spitzer,¹⁸ and shown by Chew, Goldberger, and Low,¹⁹ a large magnetic field has, under certain conditions, an effect similar to the usual collisions. Let us consider a magnetic field such as

$$\begin{aligned} \omega &\ll \omega_c, \\ qR &\ll 1, \end{aligned} \quad (\text{A10})$$

where ω_c is the cyclotron frequency and R the Larmor radius. Under such assumptions, in a plane perpendicular to the magnetic field direction, particle velocities are isotropically distributed, since the cyclotron frequency is much greater than the wave frequency, and the particles see spatial variations of the electric field only over a distance R smaller than the wavelength.

The cyclotron frequency is then equivalent to a collision frequency and the Larmor radius to a mean

free path. On the other hand, the motion parallel to \vec{B} is free and the mean drift velocity can be much greater than the phase velocity component parallel to \vec{B} , which is the Landau damping regime. However, as long as the phase velocity along \vec{B} is greater than the carriers' velocity, this difficulty disappears and one may use a hydrodynamic description. The concepts of "frozen" flux, and of kinetic and magnetic pressure can then be applied. For a propagation perpendicular to the magnetic field, one can then show the existence of the Alfvén compressional mode and its coupling with the acoustical mode, as the conducting fluid case can be transposed to the collisionless plasma case. However, it is important to point out that the problem is now two dimensional (cf. Ref. 18, pp. 17, 18, 26), and that therefore the adiabatic compressibility coefficient γ has, for the collisionless plasma, the value $\gamma = 2$ instead of $\frac{5}{3}$ for the conducting fluid.

We must point out that, from a mechanical point of view, compressional Alfvén mode and acoustical mode are essentially longitudinal modes, as matter is displaced parallel to the propagation direction.

We now discuss the case of a collisionless plasma in the limit of zero magnetic field,

$$\omega_c \ll \omega. \quad (\text{A11})$$

Tonks and Langmuir²⁰ have described the oscillation spectrum of a plasma with two types of charge carriers. The spectrum has two branches: an optical one at the plasma frequency, and a low-frequency branch with an acousticlike dispersion relation, which is therefore called the acoustic branch. In the following discussion, we only consider the low-frequency branch.

In the hydrodynamic limit

$$\omega\tau \ll 1, \quad (\text{A12})$$

$$q(v)\tau \ll 1,$$

we just find the acoustical mode described above. We want to point out an important physical fact. The plasma frequency is much higher than the collision frequency, and therefore, since the medium cannot support charge fluctuations, the electrons and ions (holes) gases are electrically locked. In other words, the relative diffusions of the two gases are not prevented by collisions, but by electric fields. Let us now consider the collisionless regime. For a neutral gas, density fluctuation just vanishes through diffusion and there is no propagation. On the other hand, in a compensated plasma, one easily imagines the possibility of propagation due to the electrical lock-in mechanism of the two gases. Let us imagine a charge fluctuation of the ion (hole) gas propagating with a phase velocity v_ϕ . This supposes that the mean velocity v_h of the carrier of the ion gas is smaller than v_ϕ , otherwise the density fluctuation

would be damped by diffusion. The lock-in mechanism then implies that this charge fluctuation is screened by the electron gas, but this is only possible if the mean velocity v_e of the electrons is higher than the wave phase velocity. So, under the conditions

$$v_h < v_\phi < v_e, \quad (\text{A13})$$

a mode of propagation in which the energy is alternatively transferred from the ion gas to the electron gas can exist in a binary ionized plasma. One should note then that some electrons move at the phase velocity of the wave in the direction of propagation, and that therefore the wave is Landau damped. However, in some special conditions, the Landau damping is negligible. Then the dispersion of the mode is acousticlike.

In the case of the compensated solid-state plasmas, this mode has been theoretically studied by Pines^{21,22} and Pines and Schrieffer.²² This mode has been observed in gaseous plasma²³ but not in solid-state plasmas. Conditions of observation in bismuth were discussed by McWhorter and May,³ who did not succeed in showing evidence for this mode. The negative results of their experiments can be explained by Landau-damping occurrence and above all by the difficulty of launching an essentially longitudinal electromagnetic mode with the transverse excitations necessarily used at the frequencies concerned. The application of a small (such as $\omega_c < \omega$) magnetic field transverse to the wave vector should diminish Landau damping, but above all should create a transverse coupling.

We now use the theory developed in Sec. II to discuss the physical nature of the Alfvén and magnetoacoustic mode from an electromagnetic point of view. We will present the phenomena of propagation in terms of equivalent electrical circuit.

In vacuum electromagnetic propagation, energy is alternatively stored under electric and magnetic form or, by analogy, under capacitive and inductive

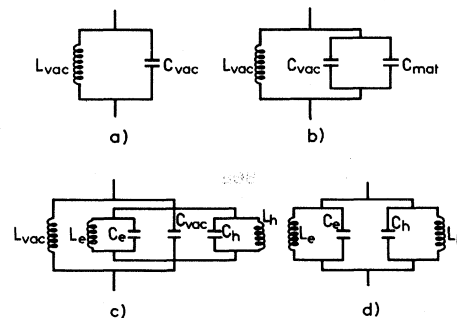


FIG. 14. Equivalent electrical circuits for propagation of (a) electromagnetic wave in vacuum; (b) compressional Alfvén wave; (c) coupled Alfvén and magnetoacoustic wave; (d) magnetoacoustic wave.

form. The vacuum capacitance C_{vac} and inductance L_{vac} are, respectively, proportional to ϵ_0 and μ_0 . The dispersion equation is then analogous to the resonance equation of a parallel L - C circuit [Fig. 14(a)].

When the electromagnetic field interacts with matter, there exists a current density \vec{j}_{mat} in parallel to the vacuum polarization (or displacement) current density \vec{j}_{dis} . In the low-frequency limit ($\omega \ll \omega_p$, where ω_p is the plasma frequency),

$$\vec{j}_{dis} \ll \vec{j}_{mat}. \quad (A14)$$

For a compensated plasma, under conditions (1),

$$\vec{j}_{mat} = \left[\sum_i \left(\frac{ne^2}{m_i} \frac{-i\omega}{\omega_{ci}^2} - \frac{2}{5} \frac{1}{-i\omega} q^2 R_i^2 \right) \right] \vec{E}. \quad (A15)$$

In the high-magnetic-field limit ($P_m > P_c$), the non-local term is negligible. It follows from (A15) that matter impedance is capacitive. Then, the Alfvén current is a polarization current, just like the vacuum displacement current, which explains the propagation mechanism. The equivalent circuit is shown in Fig. 14(b), where C_{mat} is given by

$$C_{mat} = \sum_i (ne^2/m_i \omega_{ci}^2) = C_e + C_h.$$

Energy is alternatively stored under inductive and capacitive form, i. e., under magnetic and potential form. The energy stored under electric form (in vacuum capacity) is much weaker than under magnetic form since these energies are in the ratio $(V_\phi/c)^2$, where v_ϕ and c are the Alfvén wave velocity and the light velocity.

When the magnetic pressure becomes smaller than the kinetic pressure, the nonlocal term is no longer negligible and is in fact an inductive term [see Eq. (A15)]. The electron (hole) current flows through a capacitance C_e (C_h) and an inductance L_e (L_h) in parallel [Fig. 14(c)]. In the limit $P_c \gg P_m$, the matter inductance ($L_e + L_h$) is much smaller than the vacuum inductance L_{vac} . Just as in the local regime C_{vac} is shunted by C_{mat} , so in this region L_{vac} is shunted by L_{mat} . We just get the equivalent circuit shown in Fig. 14(d).

The energy storage is then clear: A fraction of the energy is stored in each gas and flows in turn from the capacitive to the inductive form, the remaining fraction flowing from one gas to the other. The electron-hole gases are coupled through the vacuum inductance, which stores a very weak fraction of energy compared to the matter inductance, owing to the very high intensities in the L_{mat} - C_{mat} resonant circuit. In other words, the energy given by one gas to the magnetic field is simultaneously almost entirely absorbed by the other gas. This explains how the magnetic field couples the electron and hole gases when storing only a very small fraction of energy. As in the previous case, the elec-

tric energy is negligible.

In summary, the magnetohydrodynamic presentation gives us a description of the wave in the regime $P_c \gg P_m$ in terms of acoustic wave, the energy flowing in turn from the kinetic form to the potential form. The electromagnetic presentation allows us to understand how the electron and hole gases are coupled through the electromagnetic field, though the propagation mechanism is no longer electromagnetic, and gives us a physical idea of the mechanism of propagation: The energy flows alternatively from one gas to the other. This mode is a collective mode of the electron-hole plasma. In the case of the acoustic mode, described by Tonks and Langmuir,²⁰ the energy flows between the electron gas and the hole gas through the residual longitudinal electric field, while in the case of the magnetoacoustic mode it does so through the transverse electromagnetic field.

In summary, we present in Fig. 15 the different modes of propagation one can obtain in conducting matter, either conducting fluid or collisionless plasma, as a function of the magnetic field. The properties of the collisionless plasma in the cyclotron-resonance regime have been briefly reviewed in Sec. II. A theoretical study shows the coupling of the Alfvén wave with the hybrid longitudinal mode, and with nonlocal wave such as transverse and longitudinal cyclotron modes⁹ (cf. Fig. 1). In the regime where the kinetic pressure is larger than the magnetic one, the acoustic mode of the conducting fluid yields two acousticlike modes in the collisionless limit, one in the regime $\omega_c \ll \omega$, the other in the regime $\omega_c \gg \omega$. In the conducting fluid, the energy is transferred in turn from the kinetic form to the potential form, in the collisionless plasma from the electron gas to the ion gas, and vice-versa. In the regime $P_m \gg P_c$, one finds in both cases an electromagnetic mode, the com-

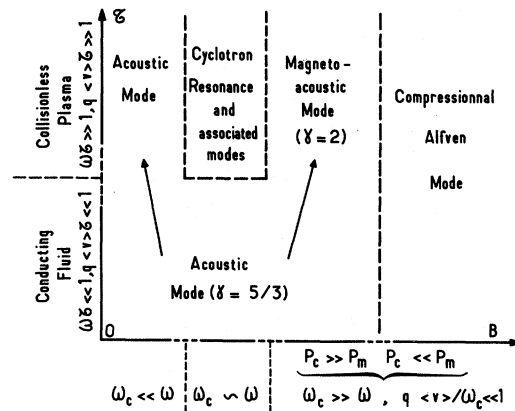


FIG. 15. Schematic diagram showing the evolution with B and τ of the different modes for a conducting fluid and a collisionless plasma.

pressional Alfvén mode. We note that the existence of the acoustic mode and of the Alfvén mode does not depend critically on the value of $\omega\tau$. This corresponds to the fact that the total momentum of a binary plasma is invariable by collisions. (This conclusion is not valid for a solid-state plasma where the momentum relaxes essentially to the lattice.)

APPENDIX B

We give here the expression of the conductivity tensor for an ellipsoidal Fermi surface $\overline{\sigma}^E(\omega, \omega_c, \vec{q})$ in terms of the conductivity tensor for a spherical Fermi surface $\overline{\sigma}^S(\omega, \omega_c, \vec{q})$. For an arbitrary Fermi surface, the integral expression of the conductivity tensor is

$$\begin{aligned} \sigma_{ij}(\vec{q}, \omega, \vec{B}) &= \frac{2e^2}{h^3} \int d\vec{p}_\pi \frac{m_c(\epsilon_F, \vec{p}_\pi)}{\omega_c} \\ &\times \int_0^{2\pi} d\phi v_i(\epsilon_F, \vec{p}_\pi, \phi) \int_{-\infty}^{\infty} d\phi' v_j(\epsilon_F, \vec{p}_\pi, \phi') \\ &\times \exp\left(\frac{\nu - i\omega}{\omega_c}(\phi' - \phi) + \frac{i}{\omega_c}\right. \\ &\left. \times \int_0^{\phi'} \vec{q} \cdot \vec{v}(\epsilon, \vec{p}_\pi, \phi'') d\phi''\right), \quad (\text{B1}) \end{aligned}$$

with standard notations.²⁴

In the case of a spherical Fermi surface, defined by the equation

$$2m_0\epsilon_F = \sum_i p_i^2$$

(where ϵ_F is the Fermi energy, m_0 the free-electron mass), for an electron at the Fermi surface in a spherical coordinates system with \vec{B} along the polar axis Oz , the Ox axis being chosen perpendicular to both \vec{q} and \vec{B} , we get

$$\begin{aligned} V_x &= (2\epsilon_F/m_0)^{1/2} \sin\theta \cos\phi, \\ V_y &= (2\epsilon_F/m_0)^{1/2} \sin\theta \sin\phi, \\ V_z &= (2\epsilon_F/m_0)^{1/2} \cos\theta, \\ p_x &= (2m_0\epsilon_F)^{1/2} \cos\theta, \\ m_c &= m_0, \\ n &= (8\pi/3h^3)(2m_0\epsilon_F)^{3/2}. \end{aligned} \quad (\text{B2})$$

From these expressions, $\overline{\sigma}^S(\omega, \omega_c, \vec{q})$ is easily derived:

$$\begin{aligned} \overline{\sigma}^S(\vec{q}, \omega, \omega_c) &= \frac{3}{2}(ne^2/m_0)(1/2\tau\omega_c) \int_0^\pi \sin\theta d\theta \int_0^{2\pi} d\phi \int_{-\infty}^{\infty} d\phi' \\ &\times \exp[\gamma(\phi' - \phi) + iqR \sin\theta (\cos\phi - \cos\phi')] \overline{\Gamma}(\theta, \phi, \phi'), \quad (\text{B3}) \end{aligned}$$

with

$$\gamma = (\nu - i\omega + iqR \nu \cos\theta)/\omega_c,$$

$$qR = q_y v_F / \omega_c,$$

$$\overline{\Gamma}(\theta, \phi, \phi') = \begin{pmatrix} \sin^2\theta \cos\phi \cos\phi' & \sin^2\theta \cos\phi \sin\phi' & \sin\theta \cos\theta \cos\phi \\ \sin^2\theta \sin\phi \cos\phi' & \sin^2\theta \sin\phi \sin\phi' & \sin\theta \cos\theta \sin\phi \\ \sin\theta \cos\theta \cos\phi' & \sin\theta \cos\theta \sin\phi' & \cos^2\theta \end{pmatrix}. \quad (\text{B4})$$

Standard double expansion in Fourier series of $\exp[iqR(\cos\phi - \cos\phi')]$ yields

$$\sigma_{ij}^S(\vec{q}, \omega, \omega_c) = \frac{3}{2} \frac{ne^2}{m_0} \sum_{p=-\infty}^{+\infty} \int_0^\pi \sin\theta d\theta \frac{W_i(p, \theta) W_j^*(p, \theta)}{\nu + i(p\omega_c - \omega + qR \nu \cos\theta)}, \quad (\text{B5})$$

with

$$W_x(p, \theta) = (1/2i) \sin\theta [J_{p-1}(\kappa) - J_{p+1}(\kappa)],$$

$$W_y(p, \theta) = \frac{1}{2} \sin\theta [J_{p-1}(\kappa) + J_{p+1}(\kappa)], \quad (\text{B6})$$

$$W_z(p, \theta) = \cos\theta J_p(\kappa),$$

where J_p is the Bessel function of order p , and κ

$= qR \sin\theta$. From Eqs. (B5) and (B6) the conductivity tensor in a small dispersion regime is easily written in a power-series expansion up to $(qR)^2$. As we are only interested in modes with electrical polarization perpendicular to the magnetic field, and with \vec{q} parallel to Oy , we just need the conductivity tensor elements in a plane perpendicular to \vec{B} . These are

$$\sigma_{xx}^i = \frac{ne^2}{m_i} \left[\frac{\nu - i\omega}{\omega_{ci}^2 + (\nu - i\omega)^2} \left(1 - \frac{3}{5} q^2 R_i^2\right) + \frac{2}{5} \frac{1}{\nu - i\omega} q^2 R_i^2 + \frac{1}{5} \frac{\nu - i\omega}{4\omega_{ci}^2 + (\nu - i\omega)^2} q^2 R_i^2 \right],$$

$$\sigma_{yy}^i = \frac{ne^2}{m_i} \left[\frac{\nu - i\omega}{\omega_{ci}^2 + (\nu - i\omega)^2} \left(1 - \frac{1}{5} q^2 R_i^2\right) + \frac{1}{5} \frac{\nu - i\omega}{4\omega_{ci}^2 + (\nu - i\omega)^2} q^2 R_i^2 \right], \quad (B7)$$

$$\sigma_{xy}^i = \frac{ne^2}{m_i} \left[\frac{\omega_{ci}}{(\nu - i\omega)^2 + \omega_{ci}^2} \left(1 - \frac{2}{5} q^2 R_i^2\right) + \frac{1}{5} \frac{2\omega_{ci}}{4\omega_{ci}^2 + (\nu - i\omega)^2} q^2 R_i^2 \right].$$

The indices i are relative to the different types of carriers (electrons and holes).

Let us now consider the case of an ellipsoidal Fermi surface defined in the right triad ($Oxyz$) by the equation

$$2m_0\epsilon_F = \alpha p_x^2 + \beta p_y^2 + \gamma p_z^2 + 2\delta p_x p_y + 2\epsilon p_y p_z + 2\zeta p_x p_z.$$

The quantities $\alpha\beta - \delta^2$ and

$$D = \begin{vmatrix} \alpha & \delta & \zeta \\ \delta & \beta & \epsilon \\ \zeta & \epsilon & \gamma \end{vmatrix}$$

are invariant under rotation around the Oz axis and under a unitary transformation, respectively.

Physically these invariances reflect the fact that these quantities are related to cyclotron mass m_c for \vec{B} along the Oz axis and to the ellipsoid volume V in momentum space, respectively:

$$m_c = m_0 / (\alpha\beta - \delta^2)^{1/2}, \quad (B8a)$$

$$V = \frac{4}{3} \pi (2m_0\epsilon_F)^{3/2} / D^{1/2}.$$

The carrier density is then

$$n = \frac{2}{h^3} V = \frac{8\pi}{3h^3} \frac{(2m_0\epsilon_F)^{3/2}}{D^{1/2}}. \quad (B8b)$$

In general, the magnetic field is not along a principal axis of the ellipsoid. The real-space trajectory is the resultant of a uniform motion along the magnetic field and of an elliptical trajectory in a plane nonperpendicular to the field (the so-called tilted cyclotron orbit). The velocity components and the momentum component p_x are

$$v_x = (2\alpha\epsilon_F/m_0)^{1/2} \sin\theta \cos(\phi - \phi_d), \quad (B8c)$$

$$v_y = (2\beta\epsilon_F/m_0)^{1/2} \sin\theta \sin\phi, \quad (B8d)$$

$$v_z = (2\eta\epsilon_F/m_0)^{1/2} \cos\theta + \mu v_x + \nu v_y, \quad (B8e)$$

$$p_x = (2m_{xx}\epsilon_F)^{1/2} \cos\theta, \quad (B8f)$$

with

$$\cos\phi_d = -(1 - \delta^2/\alpha\beta)^{1/2}, \quad (B9a)$$

$$\sin\phi_d = \delta/(\alpha\beta)^{1/2}. \quad (B9b)$$

ϕ_d just represents the fact that the principal axes of the electron elliptical orbit in a plane perpendicular to \vec{B} are not the Ox , Oy axes. The quantities η , μ , ν , are easily deduced by noting that

$$\vec{p} = \vec{m} \cdot \vec{v},$$

from which it follows that

$$v_x = p_x/m_{xx} - (m_{xz}/m_{xx})v_z - (m_{xy}/m_{xx})v_y, \quad (B10)$$

and therefore

$$\eta = D/(\alpha\beta - \delta^2),$$

$$\mu = (\beta\zeta - \epsilon\delta)/(\alpha\beta - \delta^2), \quad (B11)$$

$$\nu = (\alpha\epsilon - \zeta\delta)/(\alpha\beta - \delta^2).$$

Comparing the expressions (B8) for m_c , n , p_x , v_x , v_y , and v_z with the similar expressions (B2) for the spherical case, one easily gets the tensor $\overline{\sigma}^E \times (\omega, \omega_c, \vec{q})$ in terms of the tensor $\overline{\sigma}^S(\omega, \omega_c, \vec{q})$ with angular frequency ω_c and spatial exploration parameter qR relevant to the ellipsoid considered:

$$\omega_c = eB/m_c, \quad (B12)$$

$$qR = \frac{q_y (2\beta\epsilon_F/m_0)^{1/2}}{\omega_c}. \quad (B13)$$

We give the tensor in the case $\vec{q} \perp \vec{B}$ where the following symmetry relation holds:

$$\sigma_{xx}^S = -\sigma_{xx}^S = 0, \quad (B14a)$$

$$\sigma_{yy}^S = \sigma_{yy}^S = 0, \quad (B14b)$$

$$\sigma_{xy}^S = -\sigma_{xy}^S, \quad (B14c)$$

$$\sigma_{xx}^E = \alpha [\cos^2\phi_d \sigma_{xx}^S + \sin^2\phi_d \sigma_{yy}^S], \quad (B14d)$$

$$\sigma_{yy}^E = \beta \sigma_{yy}^S, \quad (B14e)$$

$$\sigma_{xy}^E = (\alpha\beta)^{1/2} [\cos\phi_d \sigma_{xy}^S + \sin\phi_d \sigma_{yy}^S], \quad (B14f)$$

$$\sigma_{yx}^E = (\alpha\beta)^{1/2} [\cos\phi_d \sigma_{yx}^S + \sin\phi_d \sigma_{yy}^S], \quad (B14g)$$

$$\sigma_{xx}^E = \eta \sigma_{xx}^S + \mu^2 \sigma_{xx}^E + \nu^2 \sigma_{yy}^E + \mu\nu [\sigma_{xy}^E + \sigma_{yx}^E], \quad (B14h)$$

$$\sigma_{xx}^E = \mu \sigma_{xx}^E + \nu \sigma_{xy}^E, \quad (B14i)$$

$$\sigma_{xx}^E = \mu \sigma_{xx}^E + \nu \sigma_{yx}^E, \quad (B14j)$$

$$\sigma_{yx}^E = \mu \sigma_{yx}^E + \nu \sigma_{yy}^E, \quad (B14k)$$

$$\sigma_{xy}^E = \mu \sigma_{xy}^E + \nu \sigma_{yy}^E. \quad (B14l)$$

We note the following points:

(i) σ_{yy}^E keeps the same functional form as σ_{yy}^S , while σ_{xx}^E and σ_{xy}^E do not. The physical origin is clear: The energy gained at time t by the charge

carrier,

$$\int_{-\infty}^t \vec{v}(t') \cdot \vec{E} e^{i[\alpha_y r_y(t') - \omega t']} dt',$$

is essentially dependent on the relative phase of the components of $v(t')$ and $r_y(t')$. Now, v_y and r_y keep the same relative phase whatever the Fermi surface, spherical or ellipsoidal. On the contrary, the relative phase of v_x and r_y is dependent on ϕ_d .

(ii) In the limit $qR \rightarrow 0$,

$$\sigma_{xx}^S = \sigma_{yy}^S = \frac{ne^2}{m_0} \frac{\nu - i\omega}{\omega_c^2 + (\nu - i\omega)^2}, \quad (\text{B15})$$

therefore

$$\lim_{qR \rightarrow 0} \sigma_{xx}^E = \alpha \sigma_{xx}^S.$$

(iii) In the limit $\omega_c \gg \omega$, $qR \ll 1$, we find again the usual Hall conductivity.

Since in the above limit

$$\sigma_{xy}^S \gg \sigma_{yy}^S, \quad \sigma_{xy}^S = (ne^2/m_0)(1/\omega_c), \quad (\text{B16})$$

then

$$\sigma_{xy}^E \simeq (\alpha\beta)^{1/2} \cos\phi_d \sigma_{xy}^S, \quad (\text{B17})$$

$$\sigma_{xy}^E \simeq (\alpha\beta - \delta^2)^{1/2} (m_c/m_0)(ne/B), \quad (\text{B18})$$

$$\sigma_{xy}^E \simeq ne/B. \quad (\text{B19})$$

(iv) We now demonstrate an important result, i. e., the magnetoacoustic term in σ_{xx}^E is isotropic. From Eq. (B14a), this term for an ellipsoidal Fermi surface, $\sigma_{xx}^{E \text{ nl}}$, is easily derived from the corresponding term in the spherical case, $\sigma_{xx}^{S \text{ nl}}$ (the superscript nl stands for nonlocal):

$$\sigma_{xx}^{E \text{ nl}} = \alpha \cos^2\phi_d \sigma_{xx}^{S \text{ nl}}, \quad (\text{B20})$$

$$\sigma_{xx}^{E \text{ nl}} = \alpha \cos^2\phi_d \frac{2}{5} (ne^2/m_0)(q^2 R^2/\nu - i\omega). \quad (\text{B21})$$

From Eqs. (B9a) and (B13), one gets immediately

$$\sigma_{xx}^{E \text{ nl}} = (q^2/\nu - i\omega) \frac{4}{5} (n\epsilon_F/B^2). \quad (\text{B22})$$

Thus the magnetoacoustic term is isotropic, since it depends only on the Fermi energy.

APPENDIX C

We recall here the general dispersion equation. Let Oy be the direction of propagation of an electromagnetic mode, of angular frequency ω , and wave vector \vec{q} . At low frequencies ($\omega \ll \omega_p$, plasma frequency), the current density along Oy is necessarily small because charge fluctuations cannot exist along the direction of propagation. Maxwell's equations and the medium constitutive equation $\vec{j} = \vec{\sigma} \cdot \vec{E}$ then yield

$$\begin{bmatrix} q^2 - i\mu_0\omega(\sigma_{xx} - \sigma_{xy}\sigma_{yx}/\sigma_{yy}) & -i\mu_0\omega(\sigma_{xx} - \sigma_{xy}\sigma_{yx}/\sigma_{yy}) \\ -i\mu_0\omega(\sigma_{xx} - \sigma_{xy}\sigma_{yx}/\sigma_{yy}) & q^2 - i\mu_0\omega(\sigma_{xx} - \sigma_{xy}\sigma_{yx}/\sigma_{yy}) \end{bmatrix} = 0. \quad (\text{C1})$$

Let us now suppose that the magnetic field is along the Oz axis and that the symmetry is sufficiently high so that there is no coupling (x, z) and (y, z). Then the dispersion equation (C1) factorizes and reduces to the two equations

$$q^2 = i\mu_0\omega(\sigma_{xx} - \sigma_{xy}\sigma_{yx}/\sigma_{yy}), \quad (\text{C2})$$

$$q^2 = i\mu_0\omega\sigma_{xx}. \quad (\text{C3})$$

The two proper modes are then electrically polarized, respectively, perpendicular to \vec{B} and along

\vec{B} . In fact, this is true also in a high-magnetic-field regime ($\omega_c \gg \omega$, $qR \ll 1$) for a compensated plasma. It is straightforward to show that the product of nondiagonal terms in Eq. (C1) is of the order $(\omega/\omega_c)^4$ and therefore negligible compared to the $(\omega/\omega_c)^2$ diagonal-terms products.

In conclusion, the general dispersion equation factorizes as in Eqs. (C2) and (C3) either in the case of a sufficiently high-symmetry direction or in a high-magnetic-field regime ($\omega \ll \omega_c$, $qR \gg 1$) for a compensated plasma.

¹R. T. Isaacson and G. A. Williams, Phys. Rev. **177**, 738 (1969).

²S. J. Buchsbaum and J. K. Galt, Phys. Fluids **4**, 1514 (1961).

³A. L. McWhorter and W. G. May, IBM J. Res. Develop. **8**, 285 (1964).

⁴I. Yokota, J. Phys. Soc. Japan **21**, 1851 (1966).

⁵W. L. Lupatkin and C. A. Nanney, Phys. Rev. Letters **20**, 212 (1968).

⁶J. P. D'Haenens and A. Libchaber, in *Proceedings of the Eleventh International Conference on Low-Temperature Physics*, Vol. 2, edited by J. G. Dant *et al.* (Plenum, New York, 1968), p. 1095.

⁷For a systematic experimental study of hybrid reso-

nance in bismuth, see G. E. Smith, L. C. Hebel, and S. J. Buchsbaum, Phys. Rev. **129**, 154 (1963).

⁸For cyclotron waves, see P. M. Platzman, W. M. Walsh, and E. Ni Foo, Phys. Rev. **172**, 689 (1968).

⁹The theory of the coupling of cyclotron waves and Alfvén waves has been presented by N. B. Brotsina, J. P. D'Haenens, and V. G. Skobov, Second Soviet Conference on Solid-State Physics, Moscow, 1969 (unpublished).

¹⁰R. D. Brown, R. L. Hartman, and S. H. Koenig, Phys. Rev. **598**, 172 (1968).

¹¹G. E. Smith, G. A. Baraff, and J. M. Rowell, Phys. Rev. **135A**, 1168 (1964).

¹²R. B. Lewis and T. R. Carver, Phys. Rev. **155**, 309

(1967).

¹³Montgomery, Dicke, and Purcell, *Principles of Microwave Circuits* (McGraw-Hill, New York, 1948), p. 238.

¹⁴J. Nakahara, H. Kawamura, and Y. Sawada, *Phys. Letters* **31A**, 271 (1970).

¹⁵Edelman has observed, in the same geometry, wave propagation between $\frac{1}{2}\omega_c$ and $\frac{1}{3}\omega_c$, between $\frac{1}{3}\omega_c$ and $\frac{1}{4}\omega_c$, and between $\frac{1}{4}\omega_c$ and $\frac{1}{5}\omega_c$; and the dispersion curve he obtains is well described qualitatively by the theory (Ref. 9) (private communication).

¹⁶P. A. Wolff, *Phys. Rev. B* **1**, 164 (1970).

¹⁷H. Alfvén and G. G. Falthammer, *Cosmical Electrodynamics*, 2nd ed. (Oxford U. P., London, England, 1950), p. 76.

¹⁸L. Spitzer, Jr., *Physics of Fully Ionized Gases*, 2nd ed. (Wiley, New York, 1962).

¹⁹G. F. Chew, M. L. Goldberger, and F. E. Low, *Proc. Roy. Soc. (London)* **236A**, 112 (1956).

²⁰L. Tonks and I. Langmuir, *Phys. Rev.* **33**, 195 (1929).

²¹D. Pines, *Can. J. Phys.* **34**, 1379 (1956).

²²D. Pines and J. R. Schrieffer, *Phys. Rev.* **124**, 1387 (1961).

²³E. Alexeff and R. V. Neidigh, *Phys. Rev.* **129**, 516 (1963).

²⁴E. A. Kaner and V. G. Skobov, *Advan. Phys.* **17**, 605 (1968).

Quantum-Mechanical Random-Phase-Approximation Calculation of the Surface-Plasmon Dispersion Relation for a Semi-Infinite Electron Gas*

D. E. Beck

Physics Department, University of Virginia, Charlottesville, Virginia 22901

(Received 29 March 1971)

The surface-plasmon (SPO) dispersion relation for a semi-infinite electron gas is computed for the quantum-mechanical random-phase approximation. The surface is assumed to be perfectly reflecting and the boundary-value problem is solved by a symmetric continuation of the electron gas. The linear response of the electron gas to a perturbing charge is described by a function ν which satisfies an integral equation. The integral equation for ν is solved numerically and the SPO dispersion relation is obtained by finding the pole in the density response of the electron gas to this perturbation. Graphs of the real and imaginary part of the SPO dispersion relation are given.

I. INTRODUCTION

The surface plasmon (SPO), which is a collective oscillation of the electron charge density at a surface, has recently been the object of renewed theoretical attention.¹⁻¹¹ One model of a metal surface which has been utilized in a number of these studies is a semi-infinite electron gas with a perfectly reflecting boundary. The calculations with this model²⁻⁴ have been carried out using the random-phase approximation (RPA) and an additional assumption which neglects the quantum-mechanical interference terms in the RPA (hydrodynamic or quasiclassical RPA). In this paper we report the numerical calculation of the SPO dispersion relation for a semi-infinite electron gas using the complete quantum-mechanical RPA, which represents the full exploitation of this widely used model of a metal surface. The formalism to treat this problem has already been developed^{8,12,13} and in Sec. II a brief review is presented.

The limiting long-wavelength value¹⁴ of $\omega_p/\sqrt{2}$, where ω_p is the bulk plasma frequency, has been confirmed experimentally, but there is very little direct experimental data about the dispersion relation for the SPO. The electron-energy-loss exper-

iment on Mg films¹⁵ provides a determination of the real part of the SPO frequency, $\text{Re}\omega_s(K)$, where K is the momentum parallel to the surface. The experimental values of $\text{Re}\omega_s$ for these films first decrease and then increase with increasing K .¹⁵ The RPA calculations for a semi-infinite electron gas²⁻⁴ give an $\text{Re}\omega_s$ which increases linearly with increasing K . In the present calculation, the rate of increase depends less strongly on the bulk electron density than for the hydrodynamic or quasiclassical calculations and is reduced for densities which correspond to metallic values. Two factors which contribute to the discrepancy between this experimental determination of the SPO dispersion relation and the theoretical results for a semi-infinite electron gas can be identified: The dispersion relation is more complicated for a thin film than for a single free surface,¹⁶ and, as has recently been demonstrated,^{7,17} the electron density profile at the surface is important in calculations of the SPO dispersion relation.

There are no direct experimental data for the imaginary part of the SPO frequency, $\text{Im}\omega_s(K)$, but an analysis¹⁸ of semiconductor tunnelling experiments¹⁹ provides an indication of its magnitude. The values obtained from the quasiclassical and